Aerosol dispersion in human lung: comparison between numerical simulations and experiments for bolus tests

CHANTAL DARQUENNE,[1] PETER BRAND,[2] JOACHIM HEYDER,[2] AND MANUEL PAIVA[1]
[1]Biomedical Physics Laboratory, Université Libre de Bruxelles, Brussels, Belgium;
and [2]GSF-National Research Center for Environment and Health,
Institute for Inhalation Biology, Oberschleissheim, Germany

Darquenne, Chantal, Peter Brand, Joachim Heyder, and Manuel Paiva. Aerosol dispersion in human lung: comparison between numerical simulations and experiments for bolus tests. J. Appl. Physiol. 83(3): 966–974, 1997.—Bolus inhalations of 0.87-μm-diameter particles were administered to 10 healthy subjects, and data were compared with numerical simulations based on a one-dimensional model of aerosol transport and deposition in the human lung (J. Appl. Physiol. 77: 2889–2898, 1994). Aerosol boluses were inhaled at a constant flow rate into various volumetric lung depths up to 1,500 ml. Parameters such as bolus half-width, mode shift, skewness, and deposition were used to characterize the bolus and to display convective mixing. The simulations described the experimental results reasonably well. The sensitivity of the simulations to different parameters was tested. Simulated half-width appeared to be insensitive to altered values of the deposition term, whereas it was greatly affected by modified values of the apparent diffusion in the alveolar zone of the lung. Finally, further simulations were compared in experiments with a fixed penetration volume and various flow rates. Comparison showed good agreement, which may be explained by the fact that half-width, mode shift, and skewness were little affected by the flow rate.

convective mixing; bolus inhalations; aerosol transport simulation

SEVERAL AUTHORS (8, 10, 14, 16–18) have shown that, during respiration, fresh air is irreversibly transferred from the inspired air into the surrounding air. This transfer is attributed to Brownian diffusion and convective mixing. Convective mixing refers to all the mechanisms, except Brownian diffusion, that are involved in the transfer. For example, convective mixing occurs as a result of dispersion processes, depending on such factors as velocity patterns, airway and alveolar geometry, asymmetries between inspiratory and expiratory flows, nonhomogeneous ventilation of the lung, and cardiogenic mixing. However, the contribution of each mechanism remains uncertain. Convective mixing in the lung has been measured by using the aerosol bolus technique (2, 10), whereby particles are not distributed over the entire inhaled volume but are confined within a small volume (bolus) of the inspired air. Inasmuch as ~1-μm-diameter particles have very low intrinsic motions, they act as a nondiffusing gas (1), and they may be used to trace convective and bulk processes. The bolus undergoes progressively more axial dispersion as it passes through the respiratory tract. This dispersion may be easily measured by comparing aerosol concentration curves vs. volume recorded at the mouth during inspiration and expiration. Furthermore, depending on the bolus location within the inspiratory phase, it reaches different zones of the lung and, therefore, allows a probe of convective mixing at predetermined depths within the respiratory tract.

We provide experimental data of aerosol bolus tests and compare the data with numerical simulations based on a one-dimensional model of aerosol transport and deposition within the human lung (6). Bolus inhalations to various penetration volumes were administered to 10 healthy subjects. Parameters such as bolus half-width, mode shift, skewness, and deposition are used to characterize the bolus and to display convective mixing. Numerical computations simulating the experiments are completed, and experimental and numerical data are compared. Additional experimental data obtained in 79 subjects by Brand et al. (3) are used in the comparison. The sensitivity of parameters of the numerical model is also tested.

Glossary

C	Aerosol concentration
d	Airway diameter
d_p	Particle diameter
D	Diffusion coefficient
D_a	Apparent diffusion coefficient
D_B	Brownian diffusion coefficient
DE	Particle deposition (expressed in %)
ex	Expiratory phase
FRC	Functional residual capacity
g	Gravitational acceleration
H	Bolus half-width
in	Inspiratory phase
l	Airway length
L	Total deposition function
L_d	Deposition function due to diffusion
L_i	Deposition function due to inertial impaction
L_s	Deposition function due to gravitational sedimentation
M	Bolus mode
MS	Mode shift of the bolus
$N(z)$	Number of airways in generation z
N_p	Number of particles
$N_a(z)$	Number of alveoli in generation z
Q	Flow rate
RV	Residual volume
s	Total airway cross section
s_a	Inner surface area of alveolus
S	Alveoli + airway cross section
Sk	Skewness of the bolus
St	Stokes' number ($\rho_p d_p^2 u/18\mu d$)
t	Time
TLC	Total lung capacity
u	Mean axial velocity averaged over the cross section S
u^*	Mean axial velocity averaged over the cross section s
v_s	Gravitational settling velocity
V	Volume
V_{cum}	Cumulative volume

V_p Penetration volume
x Axial coordinate
z Generation number
α Fraction of alveolated surface of airway ·
Φ_d Deposition rate by diffusion
ϕ_s Deposition rate by sedimentation
μ Dynamic viscosity of air
$\bar{\mu}$ Center of mass of the bolus
ρ_p Particle density
σ Standard deviation of the bolus

METHODS

Numerical simulation. The bolus experiments are simulated using a numerical model developed earlier by Darquenne and Paiva (6). In the simulations, a one-dimensional equation describing the aerosol transport and deposition is solved within a trumpet model based on the morphometric data of Weibel (19) and Haefeli-Bleuer and Weibel (9). This trumpet model is similar to *model C* of Darquenne and Paiva (6). The equation describing the aerosol transport and deposition along the airway path is

$$\frac{\partial C}{\partial t} = \frac{s}{S} D \frac{\partial^2 C}{\partial x^2} + \frac{1}{S} \frac{\partial(sD)}{\partial x} \frac{\partial C}{\partial x} - \frac{\dot{Q}}{S} \frac{\partial C}{\partial x} - \frac{L}{S} \quad (1)$$

with

$$D = D_B + D_a \quad (2)$$

where C is aerosol concentration, t is time, D is diffusion coefficient, s is total airway cross section, S is alveoli + airway cross section, x is axial coordinate, $\dot{Q}$ is flow rate, and L is a deposition term that incorporates deposition due to inertial impaction (L_i), gravitational sedimentation (L_s), and Brownian diffusion (L_d). These functions are listed in the APPENDIX. D incorporates Brownian diffusion (D_B) and convective mixing (D_a) and is expressed by

$$\begin{aligned} D = D_B + 2.400 \text{ cm}^2/\text{s} \quad & V_{cum} \leq 49.3 \text{ ml} \\ D = D_B + 0.167ul \quad & V_{cum} > 49.3 \text{ ml} \end{aligned} \quad (3)$$

where u is mean axial velocity in the airway and l is airway length. The first relation is used for cumulative lung volume (V_{cum}) <49.3 ml. i.e., within the oral-laryngeal path. The term 2.400 cm²/s has been used previously (6) and is examined in the DISCUSSION. The second relation is used for V_{cum} > 49.3 ml, i.e., from the entrance of the trachea down to the alveolar sacs. The term 0.167ul was proposed by Ultman (16) and corresponds to axial streaming for fully developed flow in a duct of length l. In the lung airways, the mechanisms are much more complex and involve a mixing process due to nonuniformities in the axial velocity profile in the airways. Also, for the particle size considered in this study, D_B is much smaller than D_a anywhere in the lung, except in the last generation, where $u = 0$.

The same mesh and numerical procedure described by Darquenne and Paiva (6) are used in these simulations.

Characterization of the bolus. The inhaled and exhaled boluses are characterized by the position of their mode (M) and half-width (H) on a concentration curve vs. respired volume, as defined by Heyder et al. (10). M is the volume at which the maximum aerosol concentration occurs, and H is the bolus width (in ml) between the two points of one-half the maximum concentration. The volumetric penetration (V_p) of the bolus into the lung is defined as the volume of air inhaled from the mode of the bolus to the end of the inspiratory phase.

Four parameters are used to characterize our simulations: change in H, mode shift (MS), skewness (Sk), and particle deposition (DE). H and MS are defined as differences between inhalation and exhalation data, whereas Sk is calculated from the aerosol concentration curve during expiration. The change in H reflects aerosol dispersion and is expressed as

$$H = (H_{ex}^2 - H_{in}^2)^{0.5} \quad (4)$$

where H_{in} and H_{ex} are H of the inspired and expired boluses, respectively. The MS is defined as the difference between the position of the expired bolus mode (M_{ex}) and the position of the inspired bolus (V_p)

$$MS = M_{ex} - V_p \quad (5)$$

A positive value of MS indicates that the position of the mode of the expired bolus has shifted to a larger lung volume than its location in the inhaled bolus.

Sk is computed from the expiratory curve and is expressed by

$$Sk = \frac{1}{\sigma^3} \frac{\int (V - \bar{\mu})^3 C(V) \, dV}{\int C(V) \, dV} \quad (6)$$

with

$$\bar{\mu} = \frac{\int V \, C(V) \, dV}{\int C(V) \, dV} \quad (7)$$

where V and C(V) are the volume and the aerosol concentration, respectively, and with

$$\sigma = \sqrt{\frac{\int (V - \bar{\mu})^2 C(V) \, dV}{\int C(V) \, dV}} \quad (8)$$

Finally, the percentage of deposited particles is obtained by

$$DE = \left(1 - \frac{N_{p,ex}}{N_{p,in}}\right) * 100 \quad (9)$$

where $N_{p,in}$ and $N_{p,ex}$ represent the number of inspired and expired particles, respectively. The ratio $N_{p,ex}/N_{p,in}$ is obtained by comparing the areas of the inspired and expired boluses on the plot of aerosol concentration vs. volume.

All the parameters requiring the integration of the signal are done between limits where $C(V) \geq 0.15C_{max}(V)$, inasmuch as the integration is usually done with experimental tracings to avoid errors due to the noise of the aerosol concentration signal recorded during the tests.

Breathing simulation. The first series of simulations is performed with an initial lung volume [functional residual capacity (FRC)] equal to 3 liters. The mouth-breathing cycle consists of an inspiration from FRC to 70% total lung capacity (TLC), then an expiration to residual volume (RV). The maneuver is performed at a constant flow rate of 250 ml/s. During the inspiratory phase, an aerosol bolus is injected at a preselected volume characterized by its V_p from 100 to 1,500 ml. This protocol corresponds to that performed by 10 healthy subjects (FRC = 3.5 ± 0.7 liters) in the experimental part of the study.

In the second series of simulations, V_p is fixed at 600 ml for $\dot{Q}$ from 100 to 650 ml/s. In this series the breathing cycle

consists of a 1-liter inspiration performed from FRC, then an expiration to RV.

Experimental device. The experimental setup is similar to that used by Brand et al. (4). The relevant features consist of a system of pneumatic valves connected to the mouthpiece. The system allows selection between two inhalation channels (filtered air or aerosol) and an exhaust tube for expiration. By a computer-controlled handling of the valves, an aerosol bolus can be introduced at various preselected positions within a clean air inspiration. The breathing flow rate is continuously measured with a pneumotachograph (Fleisch no. 1 tube), and the aerosol concentration is provided by a photometer. Finally, the valve system, the photometer, and the pneumotachograph are heated to prevent water condensation.

Aerosol generation. Nonhygroscopic monodisperse particles with a density of 0.91 g/cm³ are produced by heterogeneous condensation of di-2-ethyl-hexyl sebacate vapor on sodium chloride nuclei in a commercially available aerosol generator (Mage, Lavoro e Ambiente, Bologna, Italy). The aerosol is then diluted with filtered air to obtain a particle concentration of ~20,000/cm³. The diameter of the particles is 0.87 μm with a geometric standard deviation <1.15.

RESULTS

The subjects inhaled aerosol bolus into different lung depths characterized by V_p from 200 to 1,500 ml. The H of the inhaled boluses is 20 ml. Figure 1 shows examples of experimental and numerical bolus tracings at different V_p. From the experimental and numerical tracings, we characterize the bolus by means of H, MS, Sk, and DE. Figure 2 displays these parameters as a function of V_p. The experimental results obtained by Brand et al. (3) are also shown in Fig. 2. They result from bolus tests performed in 79 healthy subjects for V_p from 50 to 800 ml. In these experiments, the breathing cycle was an inspiration from FRC to 70% TLC, then an expiration to RV.

The experimental and numerical data showed a linear relationship between H and V_p, reflecting an increase in dispersion with V_p. We performed a linear curve fitting of our experimental data (V_p = 100–1,500 ml) and of the corresponding predictions from the one-dimensional model. The linear approximation was

$$H = 129 \text{ cm}^3 + 0.516 \, V_p \qquad (10)$$

for the experimental data and

$$H = 127 \text{ cm}^3 + 0.465 \, V_p \qquad (11)$$

for the numerical predictions.

The sensitivity of the numerical model to parameters such as gravity or deposition was tested. Simulations were performed by setting the gravitational acceleration to zero and then ignoring DE in the transport equation (L = 0 in *Eq. 1*). Results are shown in Fig. 2.

Simulations are also carried out by considering several levels of convective mixing in the alveolar zone of the lung (Fig. 3). First, no convective mixing is considered in the last four generations of the lung (D_a = 0). Second, in this zone a D_a equal to 10% of that used in the classical one-dimensional simulations is used (D_a = 0.1*0.167ul). Finally, computations are performed with D_a = 0.5*0.167ul. These numerical data are shown in
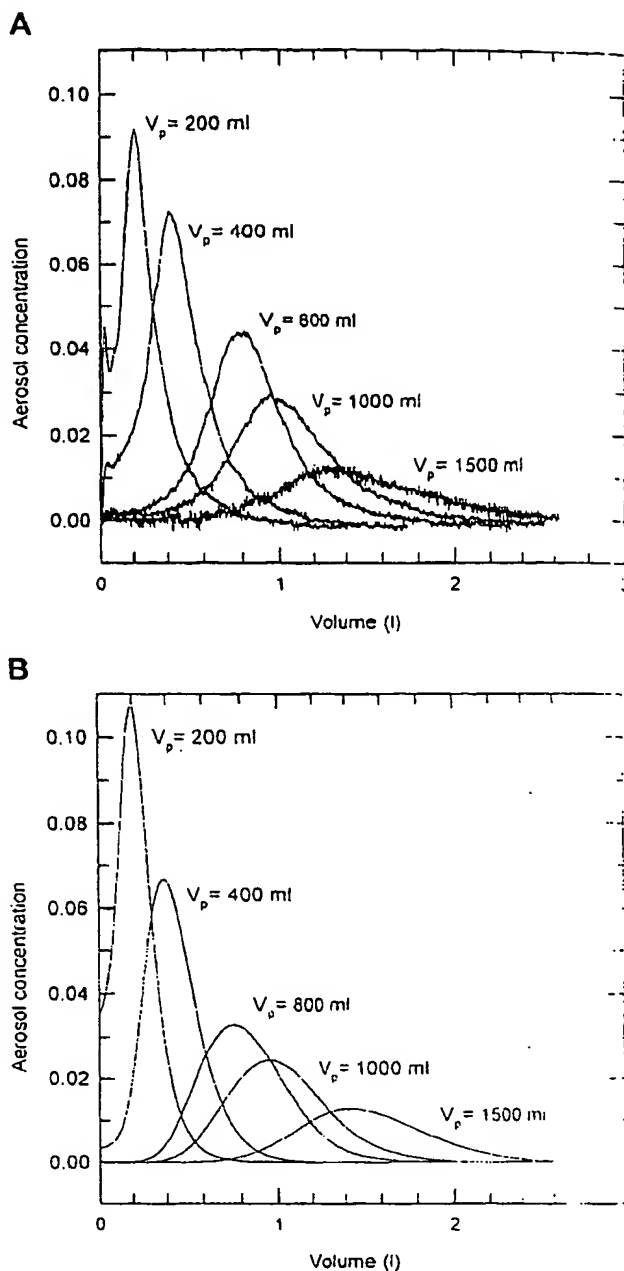
A

B

Fig. 1. Experimental tracings of 0.87-μm-diameter particles for penetration volumes (V_p) = 200, 400, 800, 1,000, and 1,500 ml; flow rate = 250 ml/s. A: experimental data from 1 subject. B: numerical data obtained from 1-dimensional model.

Fig. 3. The entrance of the last four generations corresponds to a V_p of 544 ml.

We checked the sensitivity of the bolus parameters to the threshold C ≥ 0.15C_{max}. We calculated H, MS, Sk, and DE by using a threshold of 5, 10, and 15% of C_{max}. H and MS were the same as those computed from the volume at 0.5*C_{max} and C_{max} that are above the thresholds. No significant differences were found in the com-
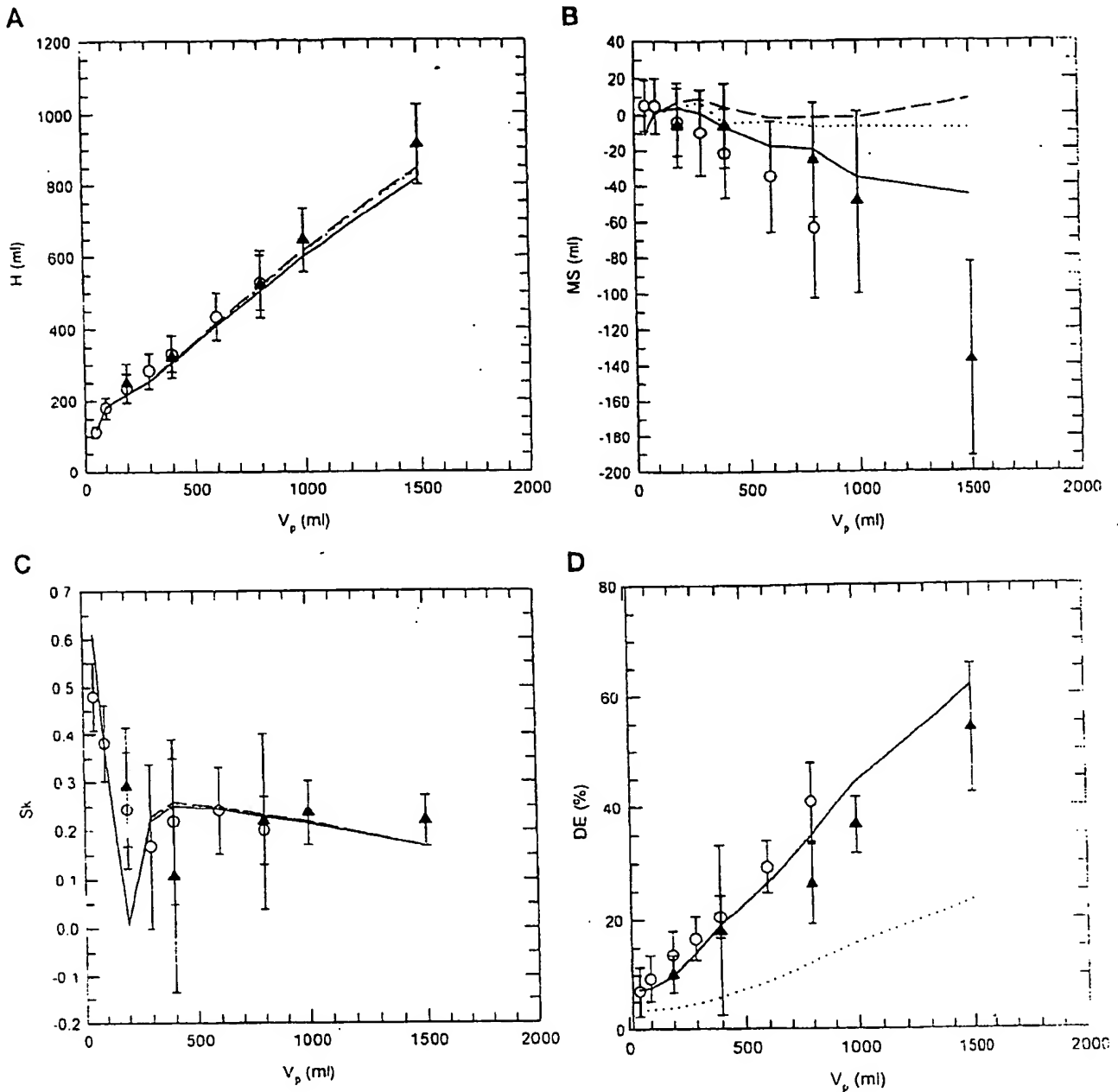
A

B

C

D

Fig. 2. Parameters characterizing aerosol bolus tracings as a function of V_p for 0.87-μm-diameter particles; flow rate = 250 ml/s. A: half-width (H). B: mode shift (MS). C: skewness (Sk). D: deposition (DE). Symbols (means $\pm$ SD) and lines refer to experimental and numerical results, respectively. ▲, Data from our 10 subjects; O, data from Brand et al. (3); solid line, reference simulations; dotted line, simulations performed at g = 0; dashed line, simulations where deposition mechanisms are neglected (L = 0).

puted DE, in contrast to Sk. The differences in Sk are displayed in Fig. 4, where the parameter is plotted as a function of V_p for the three different thresholds.

Finally, the influence of Q on aerosol dispersion is investigated in the second series of simulations. H, MS, and Sk from numerical and experimental data appear to be linearly related to Q. The linear regressions (y =

$m\dot{Q}$ + b) are displayed in Table 1. To evaluate the weight of the slope term ($m\dot{Q}$) over the intercept (b), we computed the absolute value of the ratio $m\dot{Q}/b$ for Q of 375 ml/s. The computed data are displayed in Table 1. For experimentally derived H, MS, and Sk, mean values are used in the linear regressions. The standard deviations of the experimental data are listed in Table 1. DE decreases
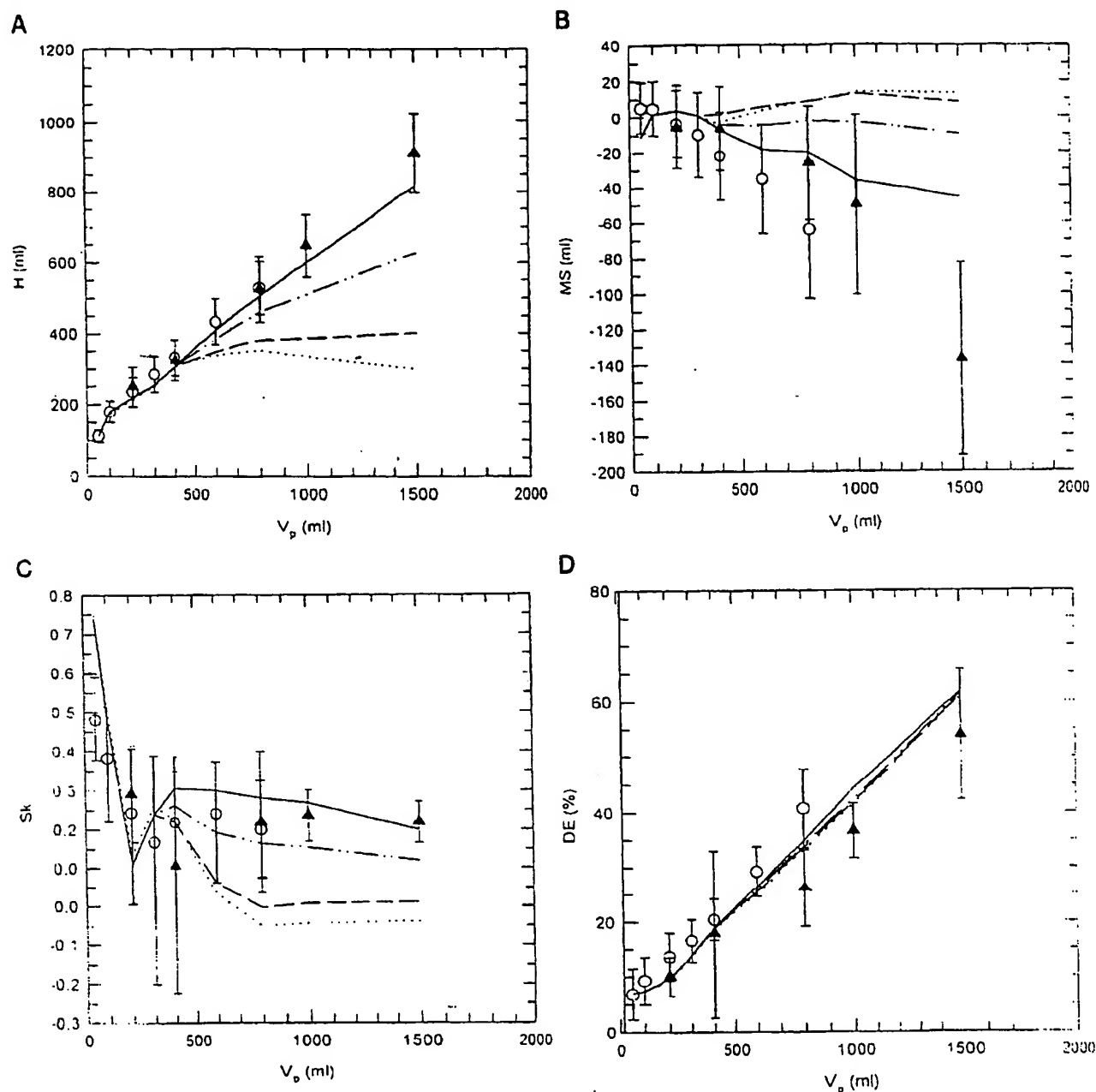
A

B

C

D

Fig. 3. Parameters characterizing aerosol bolus tracings as a function of V_p for 0.87-μm-diameter particles: flow rate = 250 ml/s. Symbols (means $\pm$ SD) and lines refer to experimental and numerical results, respectively. ▲. Data from our 10 subjects; O. data from Brand et al. (3); solid line, reference simulations; dotted line, simulations performed with apparent diffusion coefficient $(D_a) = 0$; dashed line, simulations with $D_a = 0.1 \cdot 0.167 ul$; dot-dashed line, simulations with $D_a = 0.5 \cdot 0.167 ul$. Entrance of last 4 generations corresponds to a penetration volume of 544 ml.

with increasing $\dot{Q}$. Results from numerical simulations as well as experimental data obtained from 10 subjects by Brand et al. (3) for the same protocol are shown in Fig. 5.

DISCUSSION

This study concentrates on the comparison between numerical and experimental data of aerosol dispersion

and deposition at various volumetric depths within the lung as well as the sensitivity of the simulated experiments to the different model parameters. Experimental data result from bolus inhalations administered to 10 healthy subjects. Additional experimental data of Brand et al. (3) are also considered. The numerical results are derived from one-dimensional simulations performed
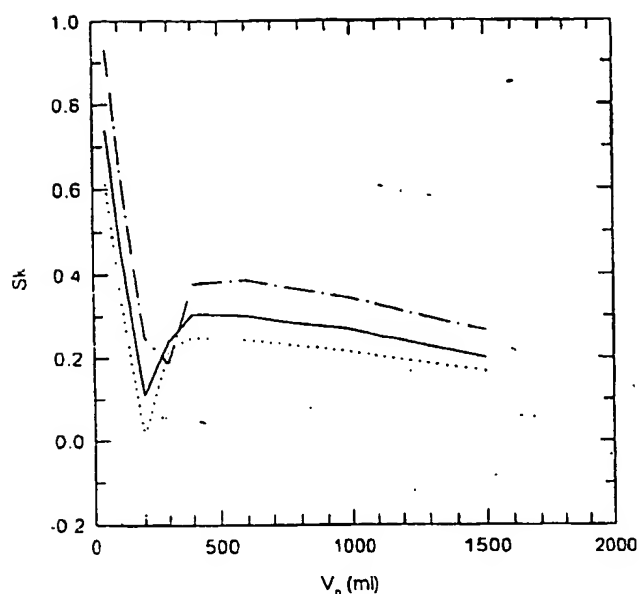
Fig. 4. Comparison between numerical Sk data (Sk_{num}) computed for different threshold of aerosol concentration (C). Dot-dashed line, $C \geq 0.05C_{max}$; solid line, $C \geq 0.10C_{max}$; dotted line, $C \geq 0.15C_{max}$.

Fig. 5. DE as a function of flow rate ($\dot{Q}$) at $V_p = 600$ ml and for 0.87-μm-diameter particles. Symbols (means $\pm$ SD), experimental data of Brand et al. (3); solid lines, numerical results.

within a trumpet model of the human lung, in which a one-dimensional equation describing aerosol transport and deposition is solved (6). As suggested previously (6), in our simulations we have considered $D_a = 2,400$ cm²/s to describe convective mixing in the oral-laryngeal path. This coefficient was chosen such that the numerical predictions fit the experimental data obtained by Anderson et al. (2) in 11 healthy subjects for $V_p = 100$-700 ml. However, we have checked the validity of this coefficient by comparing numerical and experimental tracings of bolus from three different subjects inhaling at $V_p = 40$ ml, i.e., in the oral laryngeal path (Fig. 6). The comparison shows that the use of such a dispersion coefficient in the oral-laryngeal region is acceptable.

Figure 1 illustrates the spreading of exhaled boluses for different values of V_p. Numerical tracings appear to approximate well the experimental values. The bolus is
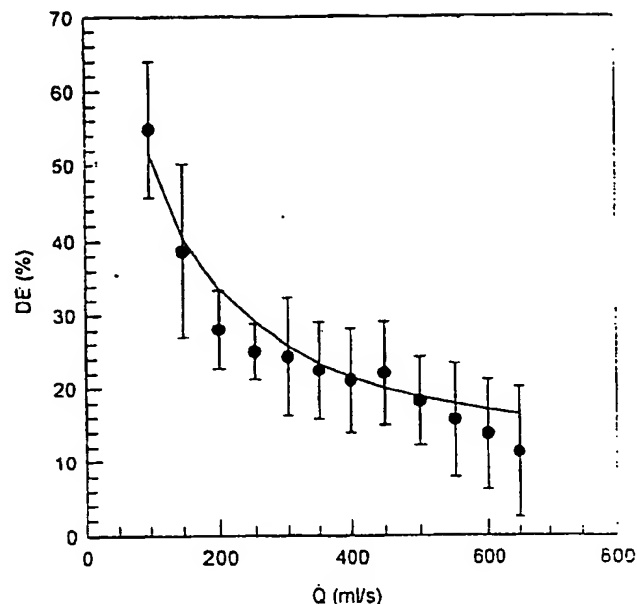
more and more dispersed as it penetrates deeper into the lung. During the inspiratory phase, the bolus divides into several segments that become more numerous as the bolus penetrates deeper into the lung. The segments recombine during expiration in such a way that the expired bolus is spread over a larger volume than the inspired bolus. This means that particles are transferred between the bolus and the surrounding air during a breath. For ~1-μm-diameter particles, intrinsic motions are very low: the diffusion coefficient is 0.3×10^{-6} cm²/s, and the settling velocity resulting

Table 1. *Linear regression of H, MS, and Sk on $\dot{Q}$*

y	$y = m\dot{Q} + b$	abs($m\dot{Q}/b$)$_{\dot{Q} = 375ml/s}$	SD_{exp}
H_{num}	$m = -7.97 \times 10^{-3}$ $b = 396.1$	7.5×10^{-3}	
H_{exp}	$m = 3.29 \times 10^{-3}$ $b = 402.5$	3.1×10^{-3}	88.8
MS_{num}	$m = 1.67 \times 10^{-2}$ $b = -20.68$	0.30	
MS_{exp}	$m = 9.60 \times 10^{-2}$ $b = -43.44$	0.83	41.87
Sk_{num}	$m = -9.86 \times 10^{-6}$ $b = 0.250$	1.5×10^{-2}	
Sk_{exp}	$m = 6.24 \times 10^{-6}$ $b = 0.151$	0.16	0.075

H, half-width (ml); MS, mode shift (ml); $\dot{Q}$, flow rate (ml/s); num, numerically determined; exp, experimentally determined.
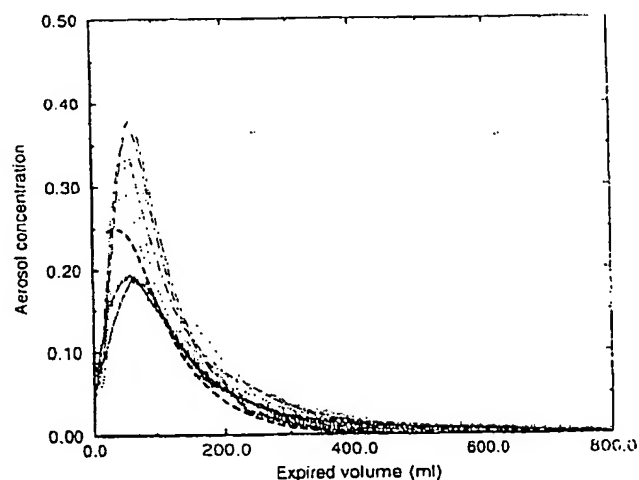

Fig. 6. Comparison between numerical and experimental tracings of expired boluses. Solid, dotted, and dot-dashed lines, experimental tracings from 3 subjects; bold dashed line, numerical tracing. Particle diameter = 0.87 μm, $\dot{Q} = 250$ ml/s, $V_p = 40$ ml.

from gravity is ~32 μm/s. In a study of convective and diffusive gas transport in canine intrapulmonary airways, Schulz et al. (12) performed aerosol bolus inhalations with 0.86- and 2.38-μm-diameter particles. They found no systematic differences between the H of the smaller and the larger particles, but the settling velocity was 7.7 times larger for 2.38- than for 0.86-μm-diameter particles. The dispersion of the bolus must therefore be attributed to mechanisms (convective mixing) other than the intrinsic particle motions.

The different parameters chosen to characterize the bolus behavior are plotted in Fig. 2 as a function of V_p. Numerical and experimental H increase continuously with V_p, indicating that each element of the lung contributes to convective mixing. Numerical values of H fit experimental data well. The linear regressions between H and V_p (*Eqs. 10* and *11*) showed a very similar intercept but a reduced slope for the numerical predictions compared with the experimental data. We also compared the linear regressions with those found by Heyder et al. (10) in a previous study performed on 17 healthy subjects. Their protocol was such that at end inspiration the subjects were at 62 or 88% of their TLC. They found

$$H = 179 \text{ cm}^3 + 0.539 \, V_p \qquad (12)$$

at the higher lung volume (88% TLC) and

$$H = 156 \text{ cm}^3 + 0.514 \, V_p \qquad (13)$$

at the lower lung volume (62% TLC). Our tests were performed at 70% TLC, and the slope of the linear regression does not show a significant difference from data of Heyder et al. The intercept is, however, lower in our experiments than in their study. As in our experiments, the data of Heyder et al. suggest a larger slope in the regression curve than that predicted from the simulations. We performed additional simulations where we modified the coefficient D_a in the alveolar zone of the lung, where its applicability is uncertain. Instead of using the function $D_a = 0.167ul$, where u is the axial velocity averaged over the total cross section S of the duct, we considered the function $D_a = ku^*$, where u^* is the axial velocity averaged over the cross section of the airways s (without the alveoli) and k is a parameter that was adjusted to obtain the best fit with the experimental data. The use of u^* instead of u was based on the two-dimensional simulations performed by Darquenne and Paiva (7) showing that the flow in the alveolar zone of the lung is mainly confined in the lumen of the airways. The best fit was obtained for $k = 0.005$ and led to the following regression curve

$$H = 100 \text{ cm}^3 + 0.542 \, V_p \qquad (14)$$

The slope of this regression curve agrees better than *Eq. 11* with the slopes derived from the experiments (*Eqs. 10, 12,* and *13*), contrary to the intercept, which is lower than previously reported.

Figure 2B displays MS. For $V_p > 100$ ml, experimental and numerical data show negative values, meaning that the bolus mode is shifted to a smaller lung volume than its location in the inspired air. This effect becomes more pronounced with increasing V_p, especially for the experimental results. Sk is displayed in Fig. 2C. Numerical and experimental data display positive values, indicating an extended tail toward the end of expiration. Moreover, Sk appears to be maximal at small V_p and tends to stabilize for larger V_p. Also, even if the curve seems to be qualitatively correct (Fig. 4), we probably underestimated Sk by using $C \ge 0.15C_{max}$, inasmuch as we excluded the contribution of a long tail. Such a high threshold was, however, chosen to minimize the parameter's dependency on the noise level of the experimental signals.

The dependence of Sk on V_p might be explained by the effect of the convective transport vs. the diffusive transport of the aerosol in the respiratory tract. In the first generations of the lung, aerosol is mainly transported by convection. During inspiration the velocity profile across the section of the airways is not uniform (11) and allows particles in the center of the ducts to reach more distal generations of the respiratory tract than particles located near the walls of the airways, where velocity is smaller. This causes a Sk of the bolus toward the distal part of the lung. During expiration, the velocity profile is more blunted (11), and particles in the center of the airways travel at a slower rate than during inspiration, whereas particles near the walls travel faster, preventing the bolus to recover its original shape. At larger V_p, this effect is attenuated by the diffusive transport, which is no longer negligible, and the exhaled bolus is more symmetrical.

Experimental and numerical deposition are compared in Fig. 2D. Deposition increases with V_p because of a longer residence time of the particles within the lung at deep V_p. Moreover, with increasing V_p, particles reach air spaces with decreasing dimensions, enhancing the probability of deposition by sedimentation and diffusion.

Further simulations have been performed with altered values of gravitational acceleration, deposition processes, or convective mixing. As shown in Fig. 2, simulated H and Sk appear to be insensitive to the removal of the gravitational force ($g = 0$) and the absence of deposition ($L = 0$), in contrast to MS. Interestingly, these results show that deposition, as simulated by the model, does not affect bolus dispersion. Total deposition seems therefore to be a poor parameter to describe the mechanisms of aerosol transport in the respiratory tract, as has been shown for a full inhalation of aerosols in previous one-dimensional simulations (6). On the other hand, simulated MS approaches zero when $g = 0$ or $L = 0$. This suggests that deposition is a determining factor in the shift of the bolus mode. This is in agreement with the results of Brown et al. (5), who performed an experimental study on dispersion of aerosol boluses in the human lung. They found a significant correlation between MS and DE: a mode shift toward the mouth (i.e., MS < 0) was associated with an increase in DE. As DE increases with increasing V_p, MS becomes more negative for deeper V_p. The removal of the gravitational force leads

to a significant decrease in DE, as expected. For 0.87-μm-diameter particles, deposition by inertial impaction is negligible, and the dotted line in Fig. 2D reflects, therefore, deposition by Brownian diffusion. The limitations of the one-dimensional model should, however, reinforce the precautions in the interpretation of these simulations. It is indeed surprising that H and Sk are very insensitive to gravitational acceleration and deposition. However, further speculation on these comparisons should await the simulations of these curves with multidimensional models.

Figure 3 illustrates that convective mixing in the alveolar zone of the lung largely affects all the parameters except deposition. The sensitivity of altered diffusion coefficient D is marked for $V_p > 400$ ml, i.e., for V_p such that the bolus may enter the alveolar zone. Darquenne and Paiva (7) studied aerosol dispersion within a two-dimensional model representative of the alveolar zone of the human lung. They discussed the validity of using the classical dispersion coefficient D_a (Eq. 3) in the one-dimensional transport equation (Eq. 1) to describe convective mixing in the alveolar zone of the lung, whereas this coefficient is based on studies performed in the first generations of the bronchial tree (16). Their simulations suggest that this coefficient may probably not be directly extended to the distal alveolar ducts, where its use overestimates mixing. Their results refer to a rather small subunit of the acinus that is ventilated synchronously. They did not take into account the effect of delays or asynchrony induced by ventilation nonuniformities between groups of acini or large lung regions, nor did they consider the chaotic mixing of flow induced by the expansion and contraction of alveolated ducts during breath (15). These effects would increase dispersion. The comparison between the linear regressions of the experiments (Eq. 10) and the numerical predictions (Eq. 11) suggest that the coefficient D_a we used in the one-dimensional model slightly underestimates convective mixing in the alveolar zone, inasmuch as we obtained a smaller slope in the linear regression of the numerical data. H is very sensitive to D_a, as shown by the different simulations displayed in Fig. 3.

Another interesting observation in Fig. 3 is that total deposition does not change significantly at any level of dispersion. Despite the fact that this parameter is too weak to allow insight into the aerosol behavior in the lung, Fig. 2D has shown that DE is sensitive to g. This suggests that experiments in hypergravity (performed in centrifuges) or in microgravity conditions, e.g., in parabolic flights or in space, can indeed shed light on the mechanisms of particle transport and deposition in the human lung.

The influence of flow rate on aerosol dispersion is displayed in Table 1 and Fig. 5. H appears to be little influenced by the flow rate, and comparison between numerical and experimental H shows good agreement. Inasmuch as experiments are performed for constant inspired and expired volumes, varying the flow rate implies a variation of the resident time of the aerosols in the respiratory tract. Convective mixing, which is primarily responsible for aerosol dispersion, is simulated in our numerical approach by a D_a proportional to the mean velocity of the gas in the airway. Furthermore, the mean displacement of particles due to diffusion may be expressed by

$$\overline{\Delta x} = \sqrt{2D_a \Delta t} \qquad (15)$$

where Δt is the mean resident time. Inasmuch as D_a is proportional to $\dot{Q}$ and Δt is inversely proportional to $\dot{Q}$, $\overline{\Delta x}$ remains constant and aerosol dispersion (i.e., H) is not influenced by $\dot{Q}$.

MS and Sk are also displayed in Table 1. Except for the experimental MS, numerical and experimental data appear to be little affected by $\dot{Q}$. If we exclude MS_{ex} at low $\dot{Q}$ (<200 ml/s), the regression parameters become $m = 1.2 \times 10^{-2}$ and $b = -2.13$, the slope of the regression line approaching that of MS_{num}. Finally, deposition decreases with increasing $\dot{Q}$, as shown on Fig. 5. The main deposition mechanism for 0.87-μm-diameter particles is gravitational sedimentation. Deposition increases therefore with increasing residence time, i.e., decreases with increasing $\dot{Q}$, as the respired volume is kept constant.

This is the third article in a series dealing with the modeling of aerosol transport and deposition in the human lung. The first article (6) dealt with one-dimensional simulations and showed that total deposition was a poor parameter to describe the aerosol behavior in the respiratory tract, although the model satisfactorily simulated the experimental data. One of the main arguments supporting this observation was the quasi-independence of total deposition on the level of convective mixing introduced in the model. The second article (7) concerned two- and three-dimensional simulations of particle transport in the alveolar zone of the lung and showed that the presence of the radial alveolar septa was a major factor in the penetration of the particles in the very periphery of the lung and that very large particle concentration inhomogeneities are expected within any acinar duct, between the lumen and the adjacent alveoli, at any moment of the respiratory cycle. The very different convective velocities in the center of the duct with respect to the adjacent alveoli were the main reason why one-dimensional models assuming uniform concentration and velocity over the cross section of the alveolar ducts cannot evaluate accurately the location of particle deposition. Here we have shown that the one-dimensional model simulates satisfactorily aerosol dispersion, which appeared to be very insensitive to gravitational acceleration and deposition. Therefore, the model as developed so far seems to be suitable to compute total deposition and dispersion of the aerosol but not to locate the sites of deposition along the respiratory tract.

In conclusion, bolus inhalations have been performed on 10 healthy subjects for various V_p. Parameters such as H, MS, Sk, and DE have been used to characterize the bolus and to display convective mixing. Numerical computations based on a one-dimensional model of aerosol transport and deposition in the human lung

have also been completed to simulate experimental tests. Even though a quite simplified approach has been used, the computations appear to describe the experimental results reasonably well. Numerical and experimental data show that irreversible processes occur in the bronchial tree, bringing about aerosol dispersion. This irreversibility of convective flow may be attributable to several factors. One factor may be differences in inspiratory and expiratory velocity gradients: during inspiration the flow divides at each bifurcation, whereas during expiration the flow continuously recombines. Nonreversible secondary flows appear at the airway bifurcations and may increase mixing. Asynchrony in the expansion and contraction of the acinar airways and also of larger ventilatory units may affect aerosol dispersion. Cardiogenic oscillations may also be responsible for mixing. Finally, additional numerical data have been compared with experimental tests performed with 10 subjects for a fixed V_p and various Q. Except for deposition, all the parameters used to describe the tests appeared to be little affected by Q.

APPENDIX

Deposition functions. The deposition term in the transport equation (*Eq. 1*) is

$$L = L_i + L_s + L_d \qquad (A1)$$

where L_i, L_s, and L_d are deposition functions due to inertial impaction, gravitational sedimentation, and Brownian diffusion, respectively. These functions are described by Darquenne and Paiva (6). The function describing deposition by inertial impaction is based on experimental data measured in a cast of the upper airways, whereas the functions of deposition by gravitational sedimentation and Brownian diffusion are derived from a theoretical approach. The functions are expressed per unit time and unit length of the airway by

$$L_i = 1.3 \frac{C\dot{Q}}{l} (St - 0.0001) \qquad St \geq 0.0001$$
$$L_i = 0 \qquad St < 0.0001 \qquad (A2)$$

for inertial impaction. where St is the Stokes' number $(\rho_p d_p^2 u / 18 \mu d)$, by

$$L_s = \frac{C\dot{Q}}{l} (1 - \alpha) \left\{ 1 - \exp\left[-2 \sqrt{\frac{N(z)}{\pi s} \frac{v_s l s}{\dot{Q}}} \right] \right\} + \phi_s \frac{N_a(z)}{l} \qquad (A3)$$

for gravitational sedimentation, and by

$$L_d = \frac{C\dot{Q}}{l} (1 - \alpha) \left\{ 1 - \exp\left[-\frac{36 D_D l N(z)}{\dot{Q}} \right] \right\} + \phi_d s_a \frac{N_a(z)}{l} \qquad (A4)$$

for diffusion, where α is fraction of alveolated surface of airway, $N(z)$ is number of airways in *generation z*, v_s is gravitational settling velocity, ϕ_s is deposition rate by sedimentation, $N_a(z)$ is number of alveoli in *generation z*, ϕ_d is deposition rate by diffusion, and s_a is inner surface of alveolus.

REFERENCES

1. Altshuler, B., E. D. Palmes, L. Yarmus, and N. Nelson. Intrapulmonary mixing of gases studied with aerosols. *J. Appl. Physiol.* 14: 321–327, 1959.
2. Anderson, P. J., J. D. Blanchard, J. D. Brain, H. A. Feldman, J. J. McNamara, and J. Heyder. Effect of cystic fibrosis on inhaled aerosol boluses. *Am. Rev. Respir. Dis.* 140: 1317–1324. 1989.
3. Brand, P., C. Rieger, H. Schulz, T. Beinert, and J. Heyder. Aerosol bolus dispersion in healthy subjects. *Eur. Respir. J.* 10: 460–467, 1997.
4. Brand, P., T. Tuch, O. Manuwald, W. Bischof, J. Heinrich. H. E. Wichmann, T. Beinert, and J. Heyder. Detection of early impairment with aerosol bolus dispersion. *Eur. Respir. J.* 7 1830–1838, 1994.
5. Brown, J. S., T. R. Timothy, W. D. Bennett, C. S. Kim, and D. E. House. Dispersion of aerosol boluses in the human lung: dependence on lung volume, bolus volume, and gender. *J. Appl. Physiol.* 79: 1787–1795, 1995.
6. Darquenne, C., and M. Paiva. One-dimensional simulation of aerosol transport and deposition in the human lung. *J. Appl. Physiol.* 77: 2889–2898, 1994.
7. Darquenne, C., and M. Paiva. Two- and three-dimensional simulations of aerosol transport and deposition in the alveolar zone of the human lung. *J. Appl. Physiol.* 80: 1401–1414, 1996.
8. Edwards, D. A. A general theory of the macrotransport of non-depositing particles in the lung by convective dispersion. *J. Aerosol Sci.* 25: 543–565, 1994.
9. Haefeli-Bleuer, D., and E. R. Weibel. Morphometry of the human pulmonary acinus. *Anat. Rec.* 220: 401–414. 1988.
10. Heyder, J., J. D. Blanchard, H. A. Feldman, and J. D. Brain. Convective mixing in human respiratory tract: estimates with aerosol boli. *J. Appl. Physiol.* 64: 1273–1278, 1988.
11. Schroter, R. C., and M. F. Sudlow. Flow patterns in models of the human bronchial airways. *Respir. Physiol.* 7: 341–355. 1969.
12. Schulz, H., P. Heilman, A. Hillebrecht, J. Gebhart, M. Meyer, J. Piiper, and J. Heyder. Convective and diffusive gas transport in canine intrapulmonary airways. *J. Appl. Physiol.* 72: 1557–1562, 1992.
13. Stahlhofen, W., L. Armbuster, J. Gebhart, and E. Grein. Particle sizing of aerosols by single particle observation in a sedimentation cell. *Atmos. Environ.* 9: 851–857. 1975.
14. Taulbee, D. B., C. P. Yu, and J. Heyder. Aerosol transport in the human lung from analysis of single breaths. *J. Appl. Physiol.* 44: 803–812, 1978.
15. Tsuda, A., F. S. Henry, and J. P. Butler. Chaotic mixing of alveolated duct flow in rhythmically expanding pulmonary acinus. *J. Appl. Physiol.* 79: 1055–1063, 1995.
16. Ultman, J. S. Gas transport in the conducting airways. In: *Gas Mixing and Distribution in the Lung*, edited by L. A. Engel and M. Paiva. New York: Dekker, 1985, vol. 25, p. 63–136. (Lung Biol. Health Dis. Ser.)
17. Ultman, J. S., B. E. Doll, R. Spiegel, and M. W. Thomas. Longitudinal mixing in pulmonary airways—normal subjects respiring at a constant flow. *J. Appl. Physiol.* 44: 297–303, 1978.
18. Ultman, J. S., and M. W. Thomas. Longitudinal mixing in pulmonary airways: comparison of inspiration and expiration. *J. Appl. Physiol.* 46: 799–805, 1979.
19. Weibel, E. R. *Morphometry of the Human Lung.* New York: Academic, 1963.